Analysis of InxGa1-xN/Si p-n heterojunction solar cells and the effects of spontaneous and piezoelectric polarization charges

AIP | Applied Physics Letters

Analysis of InxGa1−xN/Si p-n heterojunction solar cells and the effects of spontaneous and piezoelectric polarization charges

Yangdong Zheng, Akihiro Mihara, and Akio Yamamoto

Citation: Appl. Phys. Lett. **103**, 153509 (2013); doi: 10.1063/1.4824885
View online: http://dx.doi.org/10.1063/1.4824885
View Table of Contents: http://apl.aip.org/resource/1/APPLAB/v103/i15
Published by the AIP Publishing LLC.

Analysis of $In_xGa_{1-x}N$/Si *p-n* heterojunction solar cells and the effects of spontaneous and piezoelectric polarization charges

Yangdong Zheng,[1,2,3,a] Akihiro Mihara,[1,2] and Akio Yamamoto[1,2]
[1]*Department of Electrical and Electronics Engineering, Graduate School of Engineering, University of Fukui, Fukui 910-8507, Japan*
[2]*Japan Science and Technology Agency, CREST, 5 Sanbancho, Chiyoda, Tokyo 102-0076, Japan*
[3]*Center for Geo-environment Science, Graduate School of Engineering and Resource Science, Akita University, Akita 010-8502, Japan*

(Received 5 August 2013; accepted 27 September 2013; published online 11 October 2013)

The band structures, current-voltage characteristics under solar illumination, and photovoltaic (PV) properties of $In_xGa_{1-x}N$/Si *p-n* heterojunction solar cells (SCs), as well as the effects of spontaneous and piezoelectric polarization (P_{sp}-P_{PZ}) induced charges are investigated theoretically and numerically. We find that the energy peaks on the conduction and valence bands could exponentially reduce the diffusion currents and photocurrents, thus profoundly affect the PV properties of the SCs. Except for large values, the P_{sp}-P_{PZ} induced interface charges have little influence on the band structures and the PV properties. These results should be useful in analysis and design for multijunction tandem $In_xGa_{1-x}N$/Si SC devices. © *2013 AIP Publishing LLC*. [http://dx.doi.org/10.1063/1.4824885]

Recent advances in growth and doping techniques for InGaN alloys have made them an attractive candidate to realize the multijunction (MJ) tandem solar cell (SC) structures absorbing nearly the entire solar spectrum,[1–6] due to their continually tunable direct band gap spanning from 0.7 eV (InN) to 3.4 eV (GaN).[7,8] Moreover, the alloys also demonstrate many other favorable photovoltaic (PV) properties including high absorption coefficients, high carrier mobility, and saturation velocities,[9,10] as well as the superior radiation resistance.[11] On the other hand, because Si substrates are plentiful, relatively cheap, large in area and rugged, additionally, the band gap of Si (1.12 eV) is ideally suited for the bottom layer of SCs, the InGaN (top layers)/Si (bottom layer) structure is proposed to construct the SC devices.[12] The first challenge is the fabrication of *n*-$In_{0.45}Ga_{0.55}N$/*p*-Si junction SC samples by molecular beam epitaxy (MBE) a few years ago, and the measured open-circuit voltage V_{OC} was 0.46 V, short-circuit current density I_{SC} was 15.94 mA/cm^2, fill factor, FF, was 0.62, and maximum energy conversion efficiency η_{max} was merely 4.55%.[13] Although it have been predicted by theoretical studies that the energy conversion efficiencies above 30% should be achieved by 2-junction InGaN/Si SCs,[12] the experimental data of MJ InGaN/Si SCs have not been reported yet so far.

Besides the experimental techniques, such as the growth of high crystal quality InGaN layers upon Si substrates and *p* doping for rich In InGaN, the clear understanding and theoretical prediction of device parameters for gaining excellent PV characteristics are also important and effective in the challenges to fabricate the InGaN/Si SCs. Up to now, most of theoretical studies have focused on MJ structure SC models only using analytical methods available in homojunction cases.[1,2,12] However, the InGaN/Si interfaces are essentially heterojunctions, whose discontinuous band structures will affect the device transport properties. Furthermore, as group-III-nitride materials with the wurtzite crystal structure, InGaN alloys show inherent spontaneous polarizations P_{sp}.[14] Additionally, the strains in InGaN grown on Si substrates must give rise to piezoelectric polarizations P_{PZ} resulted from the lattice mismatch between InGaN and Si.[14,15] Both P_{sp} and P_{PZ} will induce interface charges and change the heterojunction band structures. The above two factors probably have substantial influence on the PV properties of the InGaN/Si SCs.

In this letter, we choose several InGaN/Si *p-n* heterojunction SC models with different In-Ga compositions and P_{sp}-P_{PZ} induced sheet charges densities in the interfaces, and carry out numerical calculations for band alignments, current-voltage (J-V) characteristics under solar illumination and typical PV properties of V_{OC}, I_{SC}, FF, and η_{max}, using derived analytical formulas based on the fluid approximation theories for semiconductor.[16–18] The results show that the *n*-InGaN/*p*-Si cells with low In contents hold higher η_{max} than that of the *n*-Si/*p*-Si cell with a similar structure. The influence of the heterojunction band structures on the PV properties of the SC devices, and the effects of the P_{sp}-P_{PZ} induced interface charges are analyzed from the theoretical viewpoint. We find that the energy peaks on the discontinue conduction band (CB) or valence band (VB), in some occasions, will exponentially reduce both the reverse saturation current densities J_{d0} and photocurrent densities J_{ph}, therefore, will remarkably affect the PV properties of the SCs. On the other hand, it seems that the P_{sp}-P_{PZ} induced interface charges do not seriously influence on the band structures and the PV properties, except in the case of large sheet charge densities. These results should be also valuable in the analysis and design for MJ tandem InGaN/Si SC devices.

We focused on *n*-$In_xGa_{1-x}N$/*p*-Si and *p*-$In_xGa_{1-x}N$/*n*-Si single junction (SJ) SC models to reveal basic features of heterojunction SCs. The band gap E_g and the electron affinity χ of Si are 1.12 and 4.05 eV, respectively.[16] The E_g

[a]Author to whom correspondence should be addressed. Electronic mail: yd_zheng@gipc.akita-u.ac.jp

of $In_xGa_{1-x}N$ with In content x was calculated by the equation $E_g = 0.7x + 3.4(1-x) - 1.43x(1-x)$ eV, with a constant bowing parameter of $b = 1.43$ eV.[2] The corresponding χ was given by $\chi = 5.8x + 4.05(1-x) + (1.43/2)x(1-x)$ eV. Incident light at AM1.5 spectral conditions illuminates on the top surface and penetrates the SC device from the InGaN top layer (layer 1) to the Si bottom layer (layer 2). The thicknesses of InGaN and Si layers were fixed at $d_1 = 0.5$ μm and $d_2 = 5000$ μm, respectively. The accepter and donor concentrations N_{A1} or N_{A2}, and N_{D1} or N_{D2} were taken equal to 1.0×10^{18} e/cm^3 for convenience of data comparisons (1.0×10^{18} e/cm^3 is the typical N_D of the n-doping InGaN films synthesized by semiconductor manufacturing processes). The Fermi levels E_{f1} and E_{f2} could be determined by $E_{fj} = -\chi_j - k_B T \ln (N_{Cj}/N_{Dj})$ [or $E_{fj} = -\chi_j - E_{gj} + k_B T \ln (N_{Vj}/N_{Aj})$], $j = 1$ or 2, where χ_j is the electron affinity, E_{gj} is the band gap, k_B is the Boltzmann constant, T is the temperature, N_{Cj} and N_{Vj} are the effective density of states (DOSs) in the conduction band and valence band, respectively.[16] We then obtained the Fermi level deference $V_D = E_{f2} - E_{f1}$. The effective dielectric constant ε_{eff} of $In_xGa_{1-x}N$ was calculated from Eq. (1) based on the Bruggeman effective medium approximation (EMA),[19] where the dielectric constants $\varepsilon_{InN} = 15.3$, $\varepsilon_{GaN} = 8.9$,

$$x\frac{\varepsilon_{InN} - \varepsilon_{eff}}{\varepsilon_{InN} + 2\varepsilon_{eff}} + (1-x)\frac{\varepsilon_{GaN} - \varepsilon_{eff}}{\varepsilon_{GaN} + 2\varepsilon_{eff}} = 0. \quad (1)$$

The basic material parameters of Si and InGaN used in calculations, including effective masses m_e and m_h ($m_{e\_Si} = 0.98$, $m_{e\_InGaN} = 0.07$, $m_{h\_Si} = 0.16$, $m_{h\_InGaN} = 0.7$ [m_0]), mobility μ_e and μ_h ($\mu_{e\_Si} = 1450$, $\mu_{e\_InGaN} = 300$, $\mu_{h\_Si} = 500$, $\mu_{h\_InGaN} = 50$ [cm^2/Vs]), Shockley-Read-Hall lifetimes τ_{SRH} ($\tau_{SRH\_Si} = \tau_{SRH\_InGaN} = 10^{-5}$ [s]), band-to-band recombination coefficients B ($B_{Si} = 4.73 \times 10^{-15}$, $B_{InGaN} = 7.5 \times 10^{-10}$ [cm^3/s]), surface recombination velocities S_e and S_h ($S_{e\_Si} = S_{e\_InGaN} = S_{h\_Si} = S_{h\_InGaN} = 10^6$ [cm/s]), etc., could be found in Ref. 12 and the literatures therein. The other parameters, such as minority carrier lifetimes τ_e and τ_h, diffusion coefficients D_n and D_p, diffusion lengths L_n and L_p, effective DOSs N_C and N_V, intrinsic carrier concentration n_i, etc., were calculated from above basic parameters.[12,16] The absorption coefficients α [μm^{-1}] used for Si and InGaN were given by[12]

$$\begin{aligned}\alpha_{Si} &= -0.425(E-E_g)^3 + 0.757(E-E_g)^2 - 0.0224(E-E_g) + 10^{-4}, \quad 1.12\,\text{eV} \le E < 1.5\,\text{eV}\\ &= 0.0287\exp[2.72(E-E_g)], \quad E \ge 1.5\,\text{eV},\end{aligned} \quad (2)$$

$$\alpha_{InGaN} = 7.91(E-E_g)^4 - 14.9(E-E_g)^3 + 5.32(E-E_g)^2 + 9.61(E-E_g) + 1.98, \quad E \ge E_g, \quad (3)$$

where E is the incident photon energy. We set reflection coefficients $R = 0$, and ignored series and shunt resistances in SCs. All the data were obtained at the temperature of 300 K.

The P_{sp} of $In_xGa_{1-x}N$ was assumed as the linear combinations of those of InN and GaN, namely, $P_{sp} = xP_{sp\_InN} + (1-x)P_{sp\_GaN}$, where $P_{sp\_InN} = \pm 2.00 \times 10^{13}$ e/cm^2, $P_{sp\_GaN} = \pm 1.81 \times 10^{13}$ e/cm^2.[20] Here, we defined the growth direction [0001] as the positive direction. The upper or lower sign (+ or −) corresponds to the N-face or III-face growth, respectively. Similarly, the lattice constant of $In_xGa_{1-x}N$ was evaluated by $a_{InGaN} = xa_{InN} + (1-x)a_{GaN}$, where $a_{InN} = 3.54$ Å, $a_{GaN} = 3.19$ Å.[20] The lattice constant of (111) plane of Si $a_{Si(111)} = 3.84$ Å calculated from $a_{Si} = 5.43$ Å.[16] Accordingly, the strain of InGaN grown on (111) plane of Si was given by $u_{xx} = a_{Si(111)}/a_{InGaN} - 1$ (tensile strain for $u_{xx} > 0$). Using the formula $P_{PZ} = 2d_{31}(c_{11} + c_{12} - 2c_{13}^2/c_{33})u_{xx}$,[15] we obtained that the P_{PZ} of $In_xGa_{1-x}N$ is in the order of $\pm 10^{15}$ e/cm^2 ($x = 0 \sim 1$), where the piezoelectric constant $d_{31} = \pm 2.0 \times 10^{-10}$ cm/V,[15,21] the elastic modulus $c_{11} = 377$, $c_{12} = 160$, $c_{13} = 114$, and $c_{33} = 209$ GPa.[22] The total polarization, $P_{tot} = P_{sp} + P_{PZ}$, being also in the order of $\pm 10^{15}$ e/cm^2. The P_{sp}-P_{PZ} induced sheet charge density at the InGaN/ Si interface can be expressed by $Q_s = -P_{tot}$. In actual devices, Q_s are usually in the order of $\pm 10^{12} \sim \pm 10^{13}$ e/cm^2, thus we selected the values in the range of $\pm 10^{12} \sim \pm 10^{15}$ for numerical calculations.

We derived analytical formulas to carry out the numerical calculations. A rigorous treatment was given for thermodynamic equilibrium states. From the standard Poisson's equations[16] and the proper boundary conditions involving Q_s, we solved the exact expressions of the Fermi level shift energies eV_{D1} and eV_{D2} as follows:

$$\begin{aligned}&(\varepsilon_1/L_{min1})\sqrt{k_{p1}[\exp(-\beta_{01}) + \beta_{01} - 1] + k_{n1}[\exp(\beta_{01}) - \beta_{01} - 1]}\\ &= (\varepsilon_2/L_{min2})\sqrt{k_{p2}[\exp(-\beta_{02}) + \beta_{02} - 1] + k_{n2}[\exp(\beta_{02}) - \beta_{02} - 1]} + Q_s,\\ &j = 1\text{ or }2, \quad \beta_{0j} = \frac{eV_{Dj}}{k_B T}, \quad V_{D1} + V_{D2} = V_D, \quad L_{pj}^2 = \frac{\varepsilon_j k_B T}{2e^2 p_{0j}}, \quad L_{nj}^2 = \frac{\varepsilon_j k_B T}{2e^2 n_{0j}},\\ &L_{minj} = \min(L_{pj}, L_{nj}), \quad k_{pj} = L_{minj}^2/L_{pj}^2, \quad k_{nj} = L_{minj}^2/L_{nj}^2,\\ &n_{0j} = \left[N_{Dj} - N_{Aj} + \sqrt{(N_{Aj} - N_{Dj})^2 + 4n_{ij}^2}\right]\Big/2, \quad p_{0j} = \left[N_{Aj} - N_{Dj} + \sqrt{(N_{Aj} - N_{Dj})^2 + 4n_{ij}^2}\right]\Big/2,\end{aligned} \quad (4)$$

where n_i is the intrinsic carrier concentration, e is the elementary charge. The internal potentials $V_1(x_1)$ and $V_2(x_2)$ were also strictly solved with an integral form as

$$\int_{\beta_{0j}}^{\beta_j} (-1)^{j+1} I(\beta_j, \beta_{0j}, k_{pj}, k_{nj}) d\beta_j = \frac{x_j - x_0}{L_{minj}}, \quad j = 1 \text{ or } 2, \quad \beta_j(x_j) = e\frac{V_j(x_j) + V_{Dj}}{k_B T}, \quad x_1 \le x_0, \quad x_2 > x_0,$$
$$I(\beta_j, \beta_{0j}, k_{pj}, k_{nj}) = \frac{1}{\sqrt{k_{pj}[\exp(-\beta_j) + \beta_j - 1] + k_{nj}[-\exp(\beta_j) - \beta_j - 1]}}, \tag{5}$$

where x_0 is the position of the interface, and x_j is the position. Then, we obtained the heterojunctions band structures (CB and VB), internal electric fields, majority and minority carrier concentrations, and space charge distributions, etc.[16–18] Because of the absence of exact solutions from the basic equations, the current densities of J_{d0} and J_{ph} in nonequilibrium states were dealt with in an approximate method as follows.[23,24] Focusing on the energy barrier peaks on the energy band (the thermodynamic equilibrium band in this letter), we denote the peak energy on the CB (VB) by E_{CB_pk} (E_{VB_pk}), the energy of p-side (n-side) flat band of CB (VB) by E_{CB_p} (E_{VB_n}), J_{d0} for electrons (holes) by J_{d0_n} (J_{d0_p}), and J_{ph} for electrons (holes) by J_{ph_n} (J_{ph_p}). If there is no energy peak existing at the interface, or $E_{CB\_p} \ge E_{CB\_pk}$ ($E_{VB\_n} \le E_{VB\_pk}$), the expressions of J_{d0} are the same as those in the homojunction cases (Ref. 16/Sec. 2.3, Ref. 17/Secs. 6.3–6.5). Otherwise, when $E_{CB\_p} < E_{CB\_pk}$ ($E_{VB\_n} > E_{VB\_pk}$), according to the diffusion theory,[23] J_{d0_n} (J_{d0_p}) derided from the homojunctions will be multiplied by an exponential function $\exp(-\Phi_b/k_BT)$, where the energy barrier $\Phi_b = E_{CB\_pk} - E_{CB\_p}$ ($\Phi_b = E_{VB\_n} - E_{VB\_pk}$). The diffusion current densities J_d are calculated from J_{d0} and $\exp(eV_b/k_BT)$, where V_b is the bias voltage. On the other hand, the photocurrent densities J_{ph} for the homojunctions can be calculated by the method described in Ref. 16/Sec. 13.9. The treatment for J_{ph_n} (J_{ph_p}) in the case of heterojunctions is similar to that for J_{d0_n} (J_{d0_p}). The calculation methods for the PV properties, such as V_{OC}, I_{SC}, FF, and η_{max}, are given by Refs. 17 and 18.

The band structure of $In_xGa_{1-x}N$/Si p-n heterojunction SCs in thermodynamic equilibrium states at typical x with $Q_s = 0$, $Q_s = \pm 10^{13}$ and $\pm 10^{15}$ e/cm^2 are illustrated in Fig. 1. We first discuss the case of n-$In_xGa_{1-x}N$/p-Si type SCs. For $x = 0.15$ in Fig. 1(a), the Fermi level $E_{f1} > E_{f2}$. When $Q_s = 0$, the Fermi level shift energies $eV_{D1} = -0.41105$ eV, $eV_{D2} = 0.34001$ eV, the depletion widths $W_1 = 27.607$ nm, $W_2 = 28.490$ nm, there is no peak on CB and VB in spite of a band energy jump at the interface. J_{d0} and J_{ph} are similar to those of homojunctions. For small $|Q_s| = 10^{13}$ e/cm^2, there is almost no change in the band shapes compared with those at $Q_s = 0$. When $|Q_s|$ becomes the large value of 10^{15} e/cm^2, the band shapes are changed seriously, but it do not affect J_{d0} and J_{ph} because of no energy peak on CB and VB. As x reaches a critical value of 0.45 in Fig. 1(b), where $E_{f1} \approx E_{f2}$, the CB and VB are flattest, and there is no peak on them. When $Q_s = 0$, $eV_{D1} = -0.07099$ eV, $eV_{D2} = 0.06928$ eV, $W_1 = 16.104$ nm, $W_2 = 15.722$ nm. The basic features of the $x = 0.45$ case are similar to those of the $x = 0.15$ case, except that when $Q_s = -10^{15}$ ($+10^{15}$) e/cm^2, there is a peak appeared on CB (VB), as well as $E_{CB\_p} < E_{CB\_pk}$ ($E_{VB\_n} > E_{VB\_pk}$), as shown in Figs. 1(b1)–1(b3) near the interfaces, which will reduce both J_{d0} and J_{ph}. If x is more than 0.45, as shown in Fig. 1(c) where $x = 0.60$, the relation between the Fermi levels is reversed as $E_{f1} < E_{f2}$, When $Q_s = 0$, $eV_{D1} = 0.05799$ eV, $eV_{D2} = -0.05888$ eV, $W_1 = 12.587$ nm, $W_2 = 12.576$ nm, the band structure is essentially different from that of the occasions at x $\le$ 0.45, because a peak appears on CB (VB), as well as $E_{CB\_p} < E_{CB\_pk}$ ($E_{VB\_n} > E_{VB\_pk}$), as shown in Figs. 1(c1)–1(c3) near the interfaces, hence J_{d0} and J_{ph} will be exponentially reduced compared with homojunction cases. The influences of nonzero Q_s on the band shapes are just like the case of $x = 0.15$, and the phenomenon of the reductions of J_{d0} and J_{ph} is not changed. These results are valuable for higher In contents. In the case of p-$In_xGa_{1-x}N$/n-Si type SCs, because generally $E_{f1} < E_{f2}$ for any x, the features of the band structures are similar. A typical instance of $x = 0.45$ is shown in Fig. 1(d). When $Q_s = 0$, $eV_{D1} = 1.5679$ eV, $eV_{D2} = -1.0745$ eV, $W_1 = 50.968$ nm, $W_2 = 43.537$ nm, the bands are bended seriously due to the large V_D, and the energy peaks appear on CB and VB. Since $E_{CB\_p} > E_{CB\_pk}$, J_{d0_n} and J_{ph_n} are similar to those of homojunctions, while

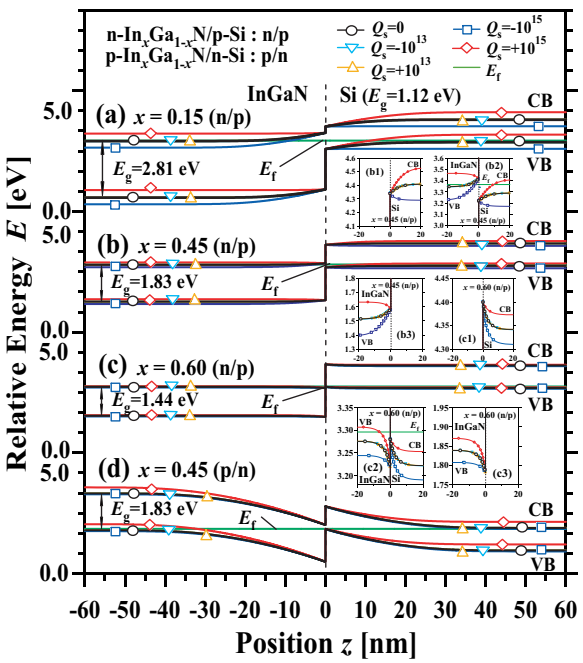

FIG. 1. Band structures of the $In_xGa_{1-x}N$/Si p-n heterojunction SC models in thermodynamic equilibrium states at various In contents x for several values of sheet charge densities Q_s in the interfaces. (a) $x = 0.15$, (b) $x = 0.45$, and (c) $x = 0.60$ for n-InGaN/p-Si junctions. (d) $x = 0.45$ for p-InGaN/n-Si junctions. Insets (b1)–(b3) and (c1)–(c3) are the enlarged views of (b) and (c) in the vicinity of the interfaces, respectively. The Fermi levels E_f are the values at $Q_s = 0$.

because $E_{VB\_n} > E_{VB\_pk}$, J_{d0_p} and J_{ph_p} will be exponentially reduced. The influences of nonzero Q_s on the band shapes also resemble the case of $x = 0.15$ of n-$In_xGa_{1-x}N$/p-Si type SCs, and the features of J_{d0_n}, J_{d0_p}, J_{ph_n}, J_{ph_p} are similar to those at $Q_s = 0$.

In Fig. 2, we demonstrate the J-V characteristics of $In_xGa_{1-x}N$/Si p-n heterojunction SCs at different x from 0 to1, with various values of Q_s under the illumination of AM 1.5G. The corresponding PV properties of V_{OC}, I_{SC}, FF, and η_{max} are shown in Fig. 3. For the n-InGaN/p-Si type SCs displayed in Figs. 2(a), 2(b) and Figs. 3(a1)–3(d1), we obtain excellent J-V characteristics and high η_{max} when $x \leq 0.45$ in the condition of $Q_s = 0$, some of them are beyond those of the n-Si/p-Si SC. The undamped I_{SC} are resulted from the fact that there is no energy peak on CB and VB, while the small J_{d0_n} in the InGaN regions (due to large E_g) lead to the large V_{OC}. However, the Ohmic characteristics are not observed even at $x = 0.45$.[12,13] As indicated in the previous paragraphs, the nonzero Q_s almost do not affect the J-V characteristics and PV properties in this case, except that when $x = 0.45$ and $Q_s = \pm 10^{15}$ e/cm^2, I_{SC} and η_{max} will be reduced due to the appearance of the energy peaks on CB and VB. Once x exceeds 0.45, the J-V characteristics and η_{max} degrade dramatically when $Q_s = 0$. I_{SC} decrease due to the

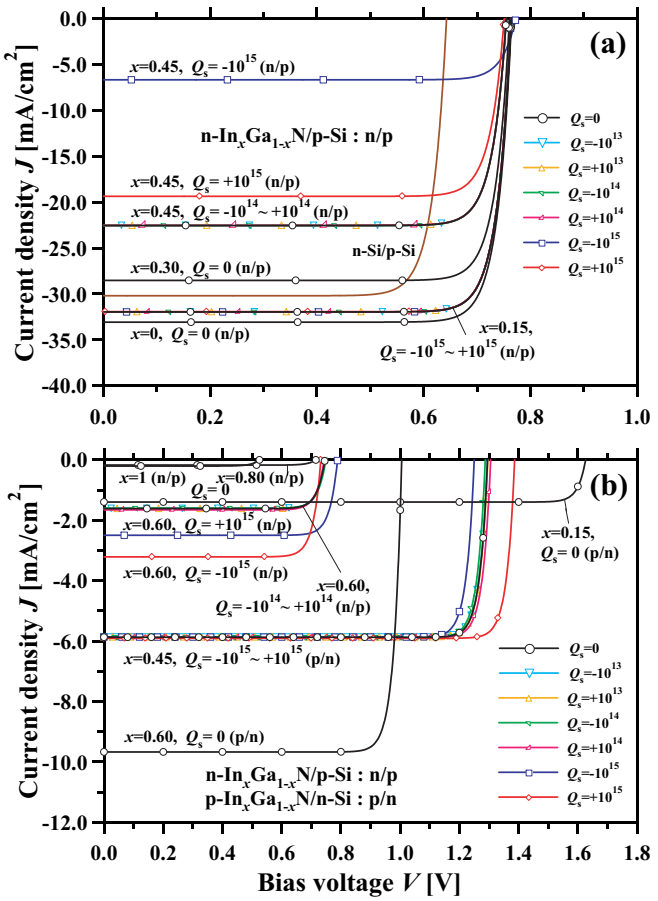

FIG. 2. J-V characteristics of the $In_xGa_{1-x}N$/Si p-n heterojunction SC models under the illumination of AM 1.5G at various In contents x for several values of sheet charge densities Q_s in the interfaces. (a) $x = 0$, 0.15, 0.30, 0.45 for n-InGaN/p-Si junctions. (b) $x = 0.60$, 0.80, 1 for n-InGaN/p-Si junctions, and $x = 0.15$, 0.45, 0.60 for p-InGaN/ n-Si junctions.

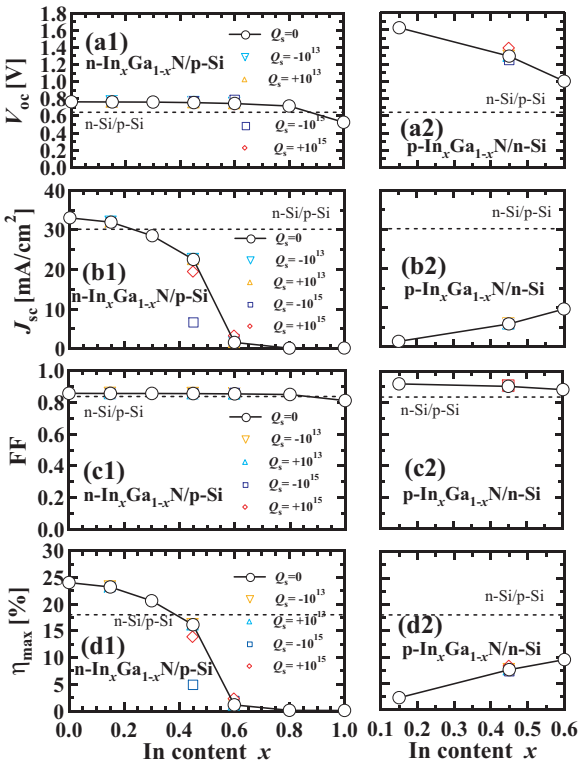

FIG. 3. The PV properties V_{OC}, I_{SC}, FF and η_{max} of the $In_xGa_{1-x}N$/Si p-n heterojunction SC models as a function of the In content x for several values of sheet charge densities Q_s in the interfaces. (a1)–(d1) n-InGaN/p-Si junctions. (a2)–(d2) p-InGaN/n-Si junctions. The dashed lines indicate the corresponding values of the n-Si/p-Si SC devices.

reductions of J_{ph} as the result of the energy peaks on CB and VB. Because both J_{ph} and J_{d0} are reduced, V_{OC} have no large changes for $V_{OC} \propto \ln(1 + J_{ph}/J_{d0})$. In the cases of nonzero Q_s, we notice that when $x = 0.60$ and $Q_s = -10^{15}$ $(+10^{15})$ e/cm^2, I_{SC} and η_{max} are improved because of the decrease of the peak energy barrier $E_{VB\_n} - E_{VB\_pk}$ (E_{CB_pk} - E_{CB_p}) and the increase of J_{ph_n} (J_{ph_p}), also see Figs. 1(c1)–1(c3). On the other hand, for the p-InGaN/n-Si type SCs displayed in Figs. 2(b), and 3(a2)–3(d2), the J-V characteristics and PV properties of different x are roughly similar. As explained in the previous paragraphs, the reduced J_{ph_p} (Si regions) will bring about the decreases of I_{SC} and η_{max}, the increases of V_{OC} are probably resulted from the reductions of J_{d0_p}, which are the dominant parts of J_{d0} (J_{ph_n} of the InGaN regions remain no change, thus $J_{ph} \approx J_{ph\_n}$ have relatively large values). The nonzero Q_s almost do not affect the J-V characteristics and PV properties in this case due to the large V_D.

In conclusion, according to the theoretical analysis, for both SJ and MJ tandem InGaN/Si p-n heterojunction SCs, the energy peaks on CB and VB could steeply reduce J_{d0} and J_{ph}, and profoundly affect the PV properties of the SCs. While Q_s have little influence on the band structures and the PV properties except for large values of Q_s. The outstanding PV properties are obtained in the n-$In_xGa_{1-x}N$/p-Si SJ SCs devices with $x \leq 0.45$.

This work was supported in part by "Creative Research for Clean Energy Generation using Solar Energy" project in

Core Research for Evolutional Science and Technology (CREST) programs of the Japan Science and Technology Agency (JST).

[1]H. Hamzaoui, A. S. Bouazzi, and B. Rezig, Sol. Energy Mater. Sol. Cells **87**, 595–603 (2005).
[2]X. B. Zhang, X. L. Wang, H. L. Xiao, C. B. Yang, J. X. Ran, C. M. Wang, Q. F. Hou, J. M. Li, and Z. G. Wang, J. Phys. D: Appl. Phys. **41**, 245104 (2008).
[3]C. J. Neufeld, N. G. Toledo, S. C. Cruz, M. Iza, S. P. DenBaars, and U. K. Mishra, Appl. Phys. Lett. **93**, 143502 (2008).
[4]M.-J. Jeng, Y.-L. Lee, and L.-B. Chang, J. Phys. D **42**, 105101 (2009).
[5]R. Dahal, B. Pantha, J. Li, J. Y. Lin, and H. X. Jiang, Appl. Phys. Lett. **94**, 063505 (2009).
[6]A. Yamamoto, Md. R. Islam, T.-T. Kang, and A. Hashimoto, Phys. Status Solidi C **7**(5), 1309–1316 (2010).
[7]J. Wu, W. Walukiewicz, K. M. Yu, J. W. Ager III, E. E. Haller, H. Lu, and W. J. Schaff, Appl. Phys. Lett. **80**, 4741 (2002).
[8]A. Schleife, F. Fuchs, C. Rodl, J. Furthmuller, and F. Bechstedt, Appl. Phys. Lett. **94**, 012104 (2009).
[9]O. Jani, I. Ferguson, C. Honsberg, and S. Kurtz, Appl. Phys. Lett. **91**, 132117 (2007).
[10]Y. Nanishi, Y. Saito, and T. Yamaguchi, Jpn. J. Appl. Phys., Part 1 **42**, 2549 (2003).
[11]J. Wu, W. Walukiewicz, K. M. Yu, W. Shan, J. W. Ager III, E. E. Haller, H. Lu, W. J. Schaff, W. K. Metzger, and S. Kurtz, J. Appl. Phys. **94**, 6477 (2003).
[12]L. Hsu and W. Walukiewicz, J. Appl. Phys. **104**, 024507 (2008).
[13]J. W. Ager, L. A. Reichertz, K. M. Yu, W. J. Schaff, T. L. Williamson, M. A. Hoffbauer, N. M. Haegel, and W. Walukiewicz1, in *Proceedings of 33rd IEEE Photovoltaic Specialists Conference, San Diego*, 11–16 May 2008.
[14]O. Ambacher, J. Smart, J. R. Shealy, N. G. Weimann, K. Chu, M. Murphy, W. J. Schaff, L. F. Eastman, R. Dimitrov, L. Wittmer, M. Stutzmann, W. Rieger, and J. Hilsenbeck, J. Appl. Phys. **85**, 3222 (1999).
[15]E. T. Yu, G. J. Sullivan, P. M. Asbeck, C. D. Wang, D. Qiao, and S. S. Lau, Appl. Phys. Lett. **71**, 2794 (1997).
[16]S. M. Sze, *Physics of Semiconductor Devices* (John Wiley & Sons, Inc., Hoboken, New Jersey, 2007).
[17]J. Nelson, *The Physics of Solar Cells* (Imperial College, London, 2003).
[18]H. J. Hovel, *Solar Cells, Semiconductors and Semimetals*, edited by A. C. Beer and R. K. Willardson (Academic, New York, 1976), Vol. 11.
[19]D. G. A. Bruggeman, Ann. Phys. (Leipzig) **24**, 636 (1935).
[20]F. Bernardini, V. Fiorentini, and D. Vanderbilt, Phys. Rev. B **56**, R10024 (1997).
[21]*Landolt-Börnstein: Numerical Data and Functional Relationships in Science and Technology*, edited by O. Madelung (Springer, New York, 1982).
[22]R. B. Schwartz, K. Khachaturyan, and E. R. Weber, Appl. Phys. Lett. **70**, 1122 (1997).
[23]R. J. Anderson, Solid State Electron. **5**, 341 (1962).
[24]L. L. Chang, Solid-State Electron. **8**, 721 (1965).